Disrupting the ciliary gradient of active Arl3 affects rod photoreceptor nuclear migration

Amanda M. Travis[1], Samiya Manocha[1], Jason R. Willer[1], Timothy S. Wessler[2], Nikolai P. Skiba[3], Jillian N. Pearring[1,4,*]

[1]Department of Ophthalmology and Visual Science, University of Michigan, Ann Arbor, MI 48105

[2]Department of Mathematics, University of North Carolina, Chapel Hill, NC 27599

[3]Department of Ophthalmology, Duke University, Durham, NC 27710

[4]Department of Cell and Developmental Biology, University of Michigan, Ann Arbor, MI 48105

[*]Correspondence: pearring@umich.edu

ABSTRACT

The small GTPase Arl3 is important for the enrichment of lipidated proteins to primary cilia, including the outer segment of photoreceptors. Human mutations in the small GTPase Arl3 cause both autosomal recessive and dominant inherited retinal dystrophies. We discovered that dominant mutations result in increased active G-protein—Arl3-D67V has constitutive activity and Arl3-Y90C is fast cycling—and their expression in mouse rods resulted in a displaced nuclear phenotype due to an aberrant Arl3-GTP gradient. Using multiple strategies, we go on to show that removing or restoring the Arl3-GTP gradient within the cilium is sufficient to rescue the nuclear migration defect. Together, our results reveal that a Arl3 ciliary gradient is involved in proper positioning of photoreceptor nuclei during retinal development.

Keywords: Arl3, photoreceptors, neuronal migration, Arl13B, RP2, retinal dystrophy

Acknowledgements: We are grateful to Mickey Kosloff (University of Haifa, Israel) for excellent feedback on the manuscript. This work was supported by a NIH P30 grant EY007003 (University of Michigan), NIH T32 grant EY013934 (A.M.T.), Matilda E. Ziegler Research Award (J.N.P.), Career Development Award (J.N.P.), an Unrestricted Grant (University of Michigan) from Research to Prevent Blindness.

Author Contributions: Conceptualization, A.M.T and J.N.P.; Methodology, A.M.T and J.N.P.; Investigation, A.M.T., S.M., J.R.W., and N.P.S.; Formal Analysis, A.M.T. and N.P.S.; Software,

T.S.W.; Writing – Original Draft, A.M.T. and J.N.P.; Writing – Review & Editing, S.M., J.R.W, N.P.S., A.M.T., and J.N.P.; Funding Acquisition, A.M.T. and J.N.P.; Supervision, J.N.P.

INTRODUCTION

Arl3 is a member of the ADP-ribosylation factor (Arf) family of small GTPases that are important for membrane trafficking (Cavenagh et al., 1994). Arl3 is ubiquitously expressed in ciliated cells where it regulates the ciliary enrichment of lipidated proteins (Fansa and Wittinghofer, 2016). Many prenylated and myristoylated proteins are shuttled by the Arl3 effectors PDEδ and UNC119A/B, respectively (Fansa et al., 2016; Zhang et al., 2011; Zhang et al., 2004). PDEδ and UNC119A/B are chaperones that sequester the lipid anchor moiety of proteins within an intramolecular cavity to enable detachment of these proteins from membranes (Hanzal-Bayer et al., 2002). Arl3 is specifically activated in the cilium by its guanine exchange factor (GEF) Arl13B and co-GEF BART (ElMaghloob et al., 2021; Gotthardt et al., 2015). Active GTP-bound Arl3 then binds to the chaperones allowing them to unload their lipidated cargo at the cilium. Arl3 is inactive outside the cilium as it is inactivated by RP2, its GTPase activating protein (GAP) (Veltel et al., 2008a; Veltel et al., 2008b) that is found enriched at the base of the cilium, although it is also present at other locations in the cell (Evans et al., 2010; Holopainen et al., 2010). Germline Arl3 knockout mice have phenotypes generally associated with human ciliopathies, including polycystic kidneys and photoreceptor degeneration (Schrick et al., 2006).

In photoreceptors, Arl3 regulates enrichment of many lipidated proteins essential for eliciting the visual response within the outer segment, a modified primary cilium (reviewed in (Frederick et al., 2020)). Recently, human mutations in Arl3 have been linked to various forms of retinal degeneration: R99I causes autosomal recessive cone-rod dystrophy (Sheikh et al., 2019), R149H or R149C cause recessive Joubert syndrome (Alkanderi et al., 2018), compound heterozygous T31A/C118F causes rod-cone dystrophy (Fu et al., 2021), Y90C causes autosomal dominant retinitis pigmentosa (Holtan et al., 2019; Strom et al., 2016), and D67V causes autosomal dominant retinal degeneration (Ratnapriya et al., 2021). The R149H/C mutation is present at the Arl3-Arl13B interface and was shown to prevent Arl3 activation by Arl13B, which causes reduced enrichment of lipidated proteins in the cilium (Alkanderi et al., 2018). Additionally, the Arl3 mutations C118F, Y90C, and D67V have also been predicted to impair its interactions with binding partners (Fu et al., 2021; Ratnapriya et al., 2021; Strom et al., 2016); while the R991, T31A, C118F, and Y90C mutations are predicted to destabilize Arl3 (Fu et al., 2021; Holtan et al., 2019; Sheikh et al., 2019). These studies predict that human disease is linked to a loss of Arl3 function; however, the fact that Arl3 mutations can present as dominant retinal dystrophy suggests that some of these variants result in excessive Arl3 activity.

Studies from mice support this idea. Both a rod-specific Arl3 knockout mouse or a transgenic mouse overexpressing constitutively active Arl3-Q71L in rods show severe retinal degeneration by 2 months and result in measurable effects on lipidated protein delivery to the outer segment (Hanke-Gogokhia et al., 2016; Wright et al., 2016). However, only mice with Arl3-Q71L transgenic expression in rods had a subset of rod nuclei displaced from the outer nuclear layer (ONL) into the inner nuclear layer (INL) (Wright et al., 2016). Rod nuclear displacement has also been observed in a RP2 knockout mouse (Li et al., 2013; Mookherjee et al., 2015), further suggesting that disrupting Arl3 activity in rods could lead to a nuclear migration phenotype. We hypothesized that the autosomal dominant human Arl3 mutations are causing constitutively active Arl3 and might result in a nuclear migration defect. Using *in vitro* biochemistry and cell-based experiments, we found that dominant Arl3 mutations, D67V and Y90C, result in increased cellular activity through distinct changes to their GTPase function. D67V is constitutively active and Y90C is fast cycling. Using *in vivo* mouse models, we further show that this aberrant activity disrupts the Arl3-GTP gradient in the cilium causing defects in rod nuclear migration. Importantly, we can rescue the migration phenotype by either removing the Arl3-GTP gradient entirely or restoring active Arl3-GTP to the cilium highlighting that the cilium is important for proper photoreceptor migration during retinal development.

RESULTS

Expression of dominant Arl3 mutants in rod photoreceptors causes nuclear mislocalization

We investigated whether the dominantly inherited human mutations of Arl3 caused a nuclear migration phenotype by expressing exogenous FLAG-tagged human Arl3-D67V and Arl3-Y90C in rods using *in vivo* electroporation. FLAG immunostaining of retinal cross-sections showed wild-type Arl3-FLAG present throughout the rod photoreceptor including, notably, within the outer segment (Fig 1A). While both Arl3-D67V-FLAG and Arl3-Y90C-FLAG expression and localization were indistinguishable from wild-type Arl3-FLAG, many of the Arl3-D67V and Arl3-Y90C nuclei were mislocalized to the INL (Fig 1B,C). This nuclear displacement is similar to transgenic expression of the GTP-locked mutant Arl3-Q71L (Wright et al., 2016) and our own electroporation of Arl3-Q71L (Fig 1D). Additionally, even the Arl3-D67V and Arl3-Y90C nuclei localized within the ONL are predominantly displaced basally, while the nuclei of wild type Arl3-FLAG rods are distributed more evenly throughout the ONL. To quantify this shift, the skewness of the gaussian distribution of FLAG-expressing nuclei within the ONL was compared between Arl3 mutants and wild type Arl3. A skewness of zero describes a normal symmetrical distribution, while negative or

positive skewness values describe a shift in the distribution apically or basally within the ONL, respectively. All the mutants that had rod nuclei mislocalized to the INL – D67V, Q71L, Y90C – were positively skewed and statistically significant from wild type (Table 1). This shift in rod nuclear position was not seen with overexpression of a GDP-bound inactive mimetic, Arl3-T31N-FLAG, suggesting that increased Arl3 activity causes a defect in rod nuclear migration (Linari et al., 1999; Fig 1E).

Arl3-Y90C is a fast cycling GTPase

Because Arl3-D67V and Arl3-Y90C phenocopied the Arl3-Q71L mislocalization of rods nuclei, we hypothesized that these mutations would also result in constitutively active Arl3. We first tested whether the Arl3 mutations are GTPase-impaired by assessing their ability to interact with the Arl3 effector PDEδ. A GST-PDEδ pull down was performed from AD293 cell lysates expressing FLAG-tagged Arl3 mutants. As expected, inactive Arl3-T31N did not bind to GST-PDEδ while the constitutively active Arl3-Q71L is bound. Arl3-D67V was also pulled down by GST-PDEδ, indicating that it is constitutively active. Surprisingly, however, Arl3-Y90C did not bind to GST-PDEδ, indicating that it is not constitutively active (Fig 2A).

To assess Arl3-Y90C's capacity to bind GTP we performed the GST-PDEδ pulldown under several different conditions. We attempted to load Arl3-Y90C with GTP by incubating Arl3-Y90C-FLAG-expressing AD293 cell lysates with EDTA (to imitate the function of the GEF by chelating out the nucleotide coordinating Mg^{2+}) and found that, if there is excess GTP in the buffer, Arl3-Y90C can bind GTP as measured by GST-PDEδ binding. In fact, Arl3-Y90C binds GTP under these nucleotide exchange promoting conditions more efficiently than the endogenous Arl3 expressed by these cells. Interestingly, when excess GTP was added Arl3-Y90C also underwent nucleotide exchange in the presence of Mg^{2+}, which blocks nucleotide exchange for endogenous Arl3 (Fig 2B). This result indicates possible GEF-independent nucleotide exchange in Arl3-Y90C, a behavior that is often described as fast cycling of a small GTPase. To confirm, we tested the behavior of Arl3-D129N (Gotthardt et al., 2015), a homologous mutant of the fast cycling Ras-D119N (Cool et al., 1999), in this assay and found it behaved biochemically identical to Arl3-Y90C (Fig 2B).

Another key component of fast cycling GTPase behavior is increased binding to the GEF due to an increased nucleotide-free state (Cool et al., 1999; Gotthardt et al., 2015). We tested whether the Arl3-Y90C mutation also caused increased binding to Arl13B, the ciliary Arl3 GEF, by analyzing the ability of FLAG-tagged Arl3 mutants to co-immunoprecipitate GFP-tagged Arl13B

from cell culture lysates. As controls we used the fast cycling D129N mutation previously shown to bind Arl13B in yeast-2-hybrid experiments (Gotthardt et al., 2015) and the Arl3-R149H mutant previously shown to disrupt interaction with Arl13B (Alkanderi et al., 2018). In Fig 2C, Western blot analysis of the FLAG eluates using an anti-GFP antibody shows Arl3-Y90C binds Arl13B. When we introduced the R149H mutation to the Arl3-Y90C mutant, Arl13B binding was disrupted similarly to the Arl3-R149H single mutant (Fig 2C), confirming that Arl3-Y90C binding to Arl13B is at the same interface as wildtype binding. This result suggests that increased Arl13B binding to the Arl3-Y90C mutant is due to an increased nucleotide-free state of Arl3-Y90C rather than fundamental alterations within its Arl13B binding site, a conclusion supported by the continued binding of Arl3-Y90C to Arl13B after an additional T31N mutation, which decouples GTP binding state from Arl13B binding behavior of Arl3-Y90C.

To confirm that these biochemical assays reveal small GTPase behavior relevant to the migration phenotype, we electroporated Arl3-D129N-FLAG in mouse rod photoreceptors and found that the fast cycling Arl3-D129N replicated the Arl3-Y90C migration phenotype (Fig 2D). Together, our data suggest that the Arl3-Y90C mutation results in fast cycling behavior that causes excess Arl3 activation *in vivo*.

Arl3-Y90C undergoes GEF-independent activation in cell culture

We next examined the nucleotide status of Arl3-Y90C in the cell. Since the fast cycling nature of Arl3-Y90C precludes any measurement of the biological nucleotide binding state using GST-PDEδ pulldowns, we incubated AD293 cells expressing wild type or mutant FLAG-tagged Arl3 constructs with the permeable crosslinker DSS and then performed FLAG immunoprecipitations to identify Arl3 effector complexes by Western blot using an anti-Arl3 antibody. As proof of concept, we performed this *in vivo* crosslinking for the inactive Arl3-T31N and constitutively active Arl3-Q71L mutants. When DSS crosslinker was added, three major Arl3 complexes were visible in the presence of active Arl3-Q71L (Fig 3A). Mass spectrometry analysis of DSS treated lysates identified three known Arl3 binding partners: RP2, UNC119, and BART in the Arl3-Q71L but not in the Arl3-T31N sample (Fig 3B).

It was previously shown that a double mutation in Arl3, E164A/D168A, reduces affinity for RP2 (Veltel et al., 2008a). To confirm that RP2 is forming the ~65 kDa complex with Arl3-Q71L in the *in vivo* crosslinking experiments, we generated and tested a Arl3-Q71L/E164A/D168A triple mutant (Q71L[noRP2]) that maintains active Arl3 binding to effectors but not RP2 (Fig 3C, lane 1). Western blot using antibodies against RP2 confirmed that the ~65 kDa band is indeed a complex between RP2 and Arl3-Q71L (Fig 3C, lane 2). We took a similar approach to confirm

that UNC119 is forming the ~55 kDa complex with Arl3-Q71L by using Arl3-D67V. This mutant has constitutive activity in our GST-PDEδ *in vitro* pull downs (Fig 2A) but is unable to interact with UNC119A-myc (Fig 3-SupFig1). Indeed, the ~55 kDa band is strongly reduced in the presence of Arl3-D67V, confirming that this complex is between Arl3 and UNC119A (Fig 3C, lane 3). We believe the final complex at ~45 kDa is between Arl3-GTP and BART but were unable to directly verify.

We then performed the *in vivo* crosslinking on cells expressing Arl3-Y90C-FLAG and found that Arl3-Y90C formed complexes with UNC119 and BART but did not make a stable complex with RP2 (Fig 3D). This result suggests that Arl3-Y90C is active in AD293 cells and binding effectors but, unlike Arl3-Q71L, is inactivated by RP2 and therefore does not form a stable complex with RP2. The fast cycling mutant Arl3-D129N showed the same pattern of Arl3 complex formation. To understand the relative level of active Arl3-Y90C in cells, we measured the band intensity of each Arl3 in complex with UNC119 or BART and normalized to the same bands in Arl3-Q71L. We found that both fast cycling mutants, Arl3-D129N and Arl3-Y90C, had significantly higher levels than wildtype Arl3 (Fig 3E). The relative amounts of effector complex formation correlate to migration phenotype: wildtype has normal migration and is not significantly different than Arl3-T31N while the amount of Arl3-Y90C and Arl3-D129N activation is closer to Arl3-Q71L, resulting in defective migration.

We also performed the *in vivo* crosslinking on cells expressing the Arl3-Y90C/R149H-FLAG double mutant construct to verify whether the aberrant activity of the fast cycling Y90C mutation is maintained in the absence of GEF binding. In Fig 3F, we see increased expression of the Arl3-UNC119 and Arl3-BART complexes in the Y90C/R149H double mutant compared to the R149H control. Importantly, the Y90C mutation no longer forms effector complexes in the presence of the T31N mutation, so binding of GTP is indeed still necessary for activity in the presence of the Y90C mutation. Together, these results confirm that GEF-independent nucleotide exchange to GTP is activating the Arl3-Y90C mutant in cells.

Our previous FLAG immunoprecipitation experiments confirmed that Arl3-Y90C has tight binding to Arl13B (Fig 2C), but to test whether this is occurring in the cell we performed *in vivo* crosslinking experiments in the presence of Arl13B-GFP. As a control, we used Arl3-R149H-FLAG and found that it was unable to form complexes with expressed with Arl13B-GFP as expected (Fig 3G). In contrast, *in vivo* crosslinking captured complexes between Arl13B-GFP and Arl3-Y90C showing that GEF binding is a feature of Arl3-Y90C in cells. We also found Arl13B-GFP complexes with Arl3-T31N/Y90C, but not with Arl3-T31N, suggesting that the Arl3-Y90C

ability to tightly bind the GEF does not depend on its nucleotide status (Fig 3G). Together our biochemical data shows that Arl3-Y90C and Arl3-Q71L both have aberrant activity and form stable complexes with important members of the Arl3 GTPase cycle, Arl13B and RP2 respectively (Fig 3H).

Aberrant Arl3 activity drives the rod nuclear migration phenotype

We hypothesized that the nuclear migration defect is caused by the aberrant activation of Arl3 within rods. If this is true, then we would expect that eliminating all Arl3 activity would allow for normal nuclear migration. We already found that the Arl3-T31N/Y90C double mutant is inactive within the cell (Fig 3F) but remains tightly bound to Arl13B (Fig 2C), which we predict would prevent activation of endogenous Arl3 in rods. To determine whether wildtype Arl3 can be activated by Arl13B in the presence of Arl3-Y90C/T31N we performed FLAG immunoprecipitations after *in vivo* crosslinking in AD293 cell co-expressing Arl13B-GFP with wildtype Arl3-FLAG and mutant Arl3-myc. We then assessed *in vivo* effector binding of the wildtype Arl3-FLAG by Western blot. We found that wildtype Arl3-FLAG is activated by Arl13B-GFP shown by presence of the UNC119 and BART complexes (Fig 4A). However, in the presence of myc-tagged Arl3-Y90C or Arl3-T31N/Y90C, the wildtype Arl3-FLAG no longer forms these effector complexes (Fig 4A). The absence of these bands is due to the Arl3-Y90C binding to Arl13B-GFP, as we see normal wild type Arl3-FLAG activation in the presence of Arl3-T31N-myc.

These results show that wild type Arl3 is unable to be activated in the presence of Arl3-Y90C confirming our working model from Fig 3H. We then expressed the Arl3-T31N/Y90C-FLAG construct in mouse rod photoreceptors to test the migration phenotype in the absence of endogenous Arl3 activation and aberrant Arl3 activity, essentially mimicking a loss of function phenotype. We found that Arl3-T31N/Y90C-FLAG did not result in a nuclear migration defect (Fig 4B), suggesting that Arl3 activity is driving the disruption of nuclear migration in rods (Fig 4C).

Increase in chaperones for lipidated proteins can rescue the Arl3-Y90C rod migration defect

Given that elevated levels of Arl3 activity within the cell lead to the migration defect, we predicted that we could rescue the phenotype by increasing the pool of available effectors essentially chelating the excess active Arl3-Y90C and/or the Arl3-Y90C bound to Arl13B. In cell culture, we find that expression of either UNC119-myc or Arl13B-GFP decreases the formation of active complexes between Arl3-Y90C-FLAG and endogenous effectors (Fig5-SupFig1). We tested this hypothesis *in vivo* by overexpressing the chaperones, UNC119 and PDEδ, with Arl3-Y90C-FLAG in mouse rods and found that rod nuclei were normally distributed throughout the ONL (Fig 5A).

Expression of these Arl3 effectors likely sequesters active Arl3-Y90C to allow for both Arl13B-dependent activation of endogenous Arl3 as well as chaperone participation in lipidated protein transport (Fig 5B).

Surprisingly, when UNC119 or PDEδ were co-expressed with Arl3-Q71L we found that rod nuclei were still mislocalized (Fig 5C). We previously observed that the level of Arl3-Q71L activity within AD293 cells was much greater than Arl3-Y90C (Fig 3D,E), so to rescue Arl3-Q71L we attempted to better match the activity level of Arl3-Y90C by switching Arl3-Q71L-FLAG from the highly expressing rhodopsin promoter to a lower expressing rhodopsin kinase promoter (Khani et al., 2007). The lower expression of Arl3-Q71L-FLAG still resulted in a rod migration defect; however, co-expression of PDEδ was now able to rescue the phenotype (Fig 5C). These data indicate that excess activation beyond a given threshold leads to an impairment in proper rod nuclear migration.

Overexpression of lipidated cargos destined for the cilium can rescue the Arl3-Y90C migration defect

We found that chaperone availability is a critical aspect of the migration defect, so we wanted to test whether adding excess lipidated cargo, thereby shifting the equilibrium of chaperone binding from Arl3-GTP to cargo, could also rescue the Arl3-Y90C phenotype. First, we co-expressed two different ciliary lipidated cargos, myc-INPP5E or NPHP3-myc, and found that they both rescued the Arl3-Y90C nuclear migration defect (Fig 6A). We also tested non-farneslyated INPP5E-C644A, which has reduced binding to PDEδ (Fig 6-SupFig1) and found that the Arl3-Y90C migration defect persisted. This lipid dependency confirms that cargo-chaperone binding is critical for rescue. Next, we tested a non-ciliary PDEδ cargo, Rnd1 (Hanzal-Bayer et al., 2002), that we confirmed binds PDEδ in a lipid-dependent manner (Fig 6-SupFig1). Interestingly, we found that co-expression of myc-Rnd1 was unable to rescue the Arl3-Y90C nuclear migration defect (Fig 6A). Together, our data shows that only ciliary, chaperone-interacting cargo rescues the migration defect, which suggests that local increases in chaperone at the cilium may restore the Arl3 gradient in the cell by directly chelating Arl3-Y90C from Arl13B allowing endogenous Arl3 to activate normally (Fig 6B).

Restoring the endogenous Arl3 cycle is sufficient for normal nuclear migration in the presence of aberrant Arl3 activity

Our results show that a Arl3-Y90C/R149H double mutant maintains aberrant activity (Fig 3F) but is unable to bind to Arl13B (Fig 2C). This double mutant allows us to directly test the importance

of the endogenous Arl3 ciliary gradient in rods since endogenous Arl3 should now be activated in the cilium by Arl13B even though aberrant activation of Arl3-Y90C/R149H will remain present throughout the cell (Fig 7A). In contrast to Arl3-Y90C, *in vivo* expression of Arl3-Y90C/R149H does not cause the migration defect, behaving similar to the Arl3-R149H single mutant (Fig 7B). So even though the presence of Arl3-Y90C/R149H has more overall Arl3 activity within rods, the consequences on nuclear migration are blunted due to a Arl3-GTP gradient in the cilium set by endogenous Arl3 interaction with Arl13B. This result underscores the importance of the ciliary gradient of active Arl3 for normal neuronal migration.

DISCUSSION

Arl3 GTPase Function

A recent flurry of papers identified multiple Arl3 variants that cause either dominant or recessive retinal disease (Alkanderi et al., 2018; Fu et al., 2021; Holtan et al., 2019; Ratnapriya et al., 2021; Sheikh et al., 2019; Strom et al., 2016). These studies highlighted the necessity of Arl3 for photoreceptor health and raised the possibly that different biochemical alterations in Arl3 might produce divergent pathobiological underpinnings. In this study, we focused on the biochemical and cellular consequences of dominant mutations in Arl3 and found that aberrant activity in rods causes a developmental nuclear migration defect. The two dominant Arl3 variants, D67V and Y90C, phenocopied the constitutively active Q71L, previously shown to result in mislocalization of rod nuclei into the INL (Wright et al., 2016). However, these dominant mutations had very different GTPase behaviors: the D67V behaved as a constitutively active GTPase and the Y90C functioned as a fast cycling GTPase.

Previous *in silico* analyses predicted that the D67V mutation would decrease affinity to the Arl3 binding partners RP2, UNC119a, and Arl13B (Ratnapriya et al., 2021). In fact, we found that Arl3-D67V forms a stable complex with RP2, like the constitutively active Q71L variant (Fig 3C); but appears to subtly change the binding properties toward the effectors PDEδ and UNC119. Even though Arl3-D67V can bind PDEδ and RP2, it does not bind them both at the same time, a Arl3-Q71L feature shown both here and previously (Fig 2-SupFig 1; Veltel et al., 2008b). We also found that that Arl3-D67V disrupted UNC119 binding (Fig 3-SupFig 1). This effector specificity is surprising considering how similar the binding interfaces are in the UNC119a-Arl2/3 and PDEδ-Arl2 crystal structures (Hanzal-Bayer et al., 2002; Ismail et al., 2012). Further study of the Arl3-D67V variant could provide insight into both the structural and functional differences between PDEδ and UNC119.

Tyrosine 90 is located right in the center of the G-domain, and this site is not strictly conserved throughout the small GTPase family. Previous predictions were that Y90C would result in haploinsufficiency due to destabilized binding to effectors or protein instability (Holtan et al., 2019; Strom et al., 2016). Instead, we discover that the Arl3-Y90C variant is behaving like a fast cycling GTPase as it has GEF-independent GTP binding (Fig 2). Our results highlight that fast cycling mutations are not just an over-active mutant — normal activation of the endogenous GTPase is also altered. We developed an easy and useful *in vivo* crosslinking assay to determine nucleotide binding state of small GTPase proteins within cells. This technique allows for a snapshot of activity that cannot be perturbed during lysis and pulldown and also provides quantitative information about effector-binding ratios. We showed that Arl3-Y90C has aberrant activity in the cells, although not as robust as Q71L, and is able to hydrolyze GTP as it does not make a stable complex with RP2 (Fig 3). Despite the higher levels of Arl3-Y90C activity in the cell, we actually find that reactivating endogenous Arl3 in the presence of this activity prevents the nuclear migration defect in rods. This suggests that the defect is not caused by an increase in overall Arl3 activity, but a disruption of proper Arl3-GTP localization within the cell.

We demonstrate that more active Arl3 must be present in the cilium than the cell body for proper migration of rod nuclei during retinal development. This requirement for a ciliary Arl3-GTP gradient seems very similar to the Ran-GTP gradient important for nuclear transport (Sorokin et al., 2007). Movement down this gradient acts as a driving force behind cargo delivery into the cilium, so altering rather than removing the Arl3 gradient would have a distinct impact on cargo behavior. When Arl3 activity levels are increased in the cell body relative to the cilium, the driving force reverses, and cargo is no longer delivered. It is possible that disrupting delivery results in downregulation of the cargo. This might explain why absence of Arl3 activity does not cause a migration defect (Fig 4), as there would be no driving force on the cargo and its widespread delivery could result in sufficient accumulation at the cilium.

Neuronal Migration

We found that mutations in Arl3 can cause a mislocalization of rod photoreceptor nuclei toward the basal ONL and into the INL. Our results show a satisfying alignment between biochemical behavior, genetic presentation, and migration phenotype; however, our studies did not address whether the migration defect caused by the aberrant Arl3 activity is sufficient to cause degeneration. The knockout of RP2, resulting in increased Arl3 activity, causes progressive photoreceptor degeneration and has a population of rods mislocalized to the INL (Li et al., 2013). However, RP2 gene therapy in adult mice slowed degeneration, suggesting that the rod nuclear

mislocalization may not be pathogenic (Li et al., 2013; Mookherjee et al., 2015). Nevertheless, it was previously shown that basal displacement of rod nuclei coincides with retinal disfunction including defects in synapse formation (Aghaizu et al., 2021; Yu et al., 2011), so even if the rod migration defect does not directly cause cell autonomous degeneration it could affect the physiological function of rods and therefore retinal health. The exact pathobiological outcomes of displaced photoreceptor nuclei remain to be fully understood.

A related question is why the two dominant mutations cause retinal degeneration but not ciliopathies. Arl3 is expressed in all ciliated cells, and some recessive Arl3 mutations do cause syndromic disease. In fact, mutations in Arl13B, the Arl3 GEF, cause the syndromic ciliopathy Joubert syndrome (Cantagrel et al., 2008) and can cause a reduction of Arl3 activation (Gotthardt et al., 2015). The Arl3 GAP RP2, on the other hand, causes non-syndromic retinal degeneration (Breuer et al., 2002), providing more evidence that the impact of excess active Arl3 on cells is more detrimental for retinal photoreceptors than other ciliated cells throughout the body. Further studies are needed to determine if the migration phenotype is present in other neurons or if the mechanism linking Arl3 function to nuclear translocation is photoreceptor specific.

Finally, while our data demonstrates that the cilium is involved in the apical nuclear translocation of rod photoreceptors, the precise ciliary signal remains unknown. Cilia have previously been shown to play a role in neuronal nuclear migration, with studies implicating both Arl13B (Higginbotham et al., 2012) and cAMP signaling (Stoufflet et al., 2020). Our study now links Arl3 to nuclear migration and the next step will be to identify the lipidated cargo relying on the ciliary Arl3 gradient within photoreceptors during development.

MATERIALS AND METHODS

Animals

Mice were handled following protocols approved by the Institutional Animal Care and Use Committees at the University of Michigan (registry number A3114-01). Albino CD-1 wild-type mice used in electroporation experiments were ordered from Charles River Laboratories (Strain # 022; Mattawan, MI). All mice were housed in a 12/12-hour light/dark cycle with free access to food and water.

DNA constructs

For rod-specific expression, sequences were cloned between 5' *AgeI* and 3' *NotI* cloning sites into a vector with of 2.2kb of the mouse rhodopsin promoter, which was originally cloned from

pRho-DsRed, a gift from Connie Cepko (Addgene plasmid #11156; http://n2t.net/addgene:11156; RRID:Addgene_11156). FLAG-tagged Arl3 was created by cloning the entire human Arl3 sequence from pDEST47-ARL3-GFP, a gift from Richard Kahn (Addgene plasmid #67397; http://n2t.net/addgene:67397; RRID:Addgene_67397) followed by a AVPVDSRGSRA linker and a C-terminal 3X FLAG sequence (Sigma-Aldrich). All mutations in Arl3 were created using PCR mutagenesis (Weiner et al., 1994). The Arl3-Q71L-FLAG was also cloned into a plasmid with the human rhodopsin kinase promoter (originally cloned from hRK:GFP AAV, a gift from Tiansen Li). For chaperone over-expression: either human PDEδ (NM_002601.4; Dharmacon MHS6278-202829730) or mouse UNC119A (NM_005148; Origene RC203758) was cloned in front of a T2A site followed by mCherry to allow for co-translational cleavage and expression. For cargo over-expression: N-terminal MYC tags were placed in front of mouse INPP5E (Fansa et al., 2016) and human Rnd1 cloned from GFP-Rnd1, a gift from Channing Der (Addgene plasmid #23227), and C-terminal MYC tag was placed in front of human NPHP3 (GeneCopoeia GC-H2370). All mutations to replace the lipidated cysteine with alanine were made using PCR mutagenesis (Weiner et al., 1994).

Every protein expressed in mouse rods was also cloned into pEGFP-N1 (Clontech) for expression in AD293 cells using the *AgeI* and *NotI* cloning sites within the vector to replace EGFP with the tagged proteins, except for UNC119A which was tagged with C-terminal MYC rather than in front of a T2A site for cell culture expression. Additionally, Arl13B was a cloned from mouse cDNA into pcDNA3-EGFP plasmid, a gift from Doug Golenbock (Addgene plasmid #13031; http://n2t.net/addgene:13031; RRID: Addgene_13031) and pEGFPN1-HA-RP2 was cloned from (Dharmacon MMM1013-202842815).

GST-PDEδ was cloned by adding human PDEδ (NM_002601.4; Dharmacon MHS6278-202829730) to an expression vector with N-terminal GST and 6XHis: pET28GST-LIC was a gift from Cheryl Arrowsmith (Addgene plasmid # 26101; http://n2t.net/addgene:26101; RRID: Addgene_26101). A complete list of primers can be found in Supplemental Table 1.

In vivo *electroporation of mouse retinas*

DNA constructs were electroporated into the retinas of neonatal mice using the protocol as originally described by (Matsuda and Cepko, 2004), but with modifications as detailed by (Pearring et al., 2015). Briefly, P0-P2 mice were anesthetized on ice, had their eyelid and sclera punctured at the periphery of the eye with a 30-gauge needle, and were injected with 0.25-0.5 µL of 2 µg/µL concentrated plasmid with 0.5 µg/µL of pRho-mCherry (Pearring et al., 2014) or pRho-eGFP-Cb5$_{TM}$ (Baker et al., 2008) as an electroporation marker in the subretinal space using a

blunt-end 32-gauge Hamilton syringe. The positive side of a tweezer-type electrode (BTX) was placed over the injected eye and five 100V pulses of 50 msec were applied using an ECM830 square pulse generator (BTX). Neonates were returned to their mother until collection at P21.

Immunofluorescence

Eyes were enucleated at P21 after sacrifice by CO2 inhalation and fixed in 4% paraformaldehyde in PBS at room temperature for 1 hour before washing with PBS. Eye cups with patches of mCherry expression were embedded in 4% agarose (Thermo Fisher Scientific, BP160-500) and cut into 100 µm thick sagittal sections. After blocking with 5% donkey serum (Thermo Fisher Scientific NC0629457) and 0.2% Triton X-100 in PBS for 1 hour at room temperature, free floating sections were incubated with mouse anti-FLAG clone M2 antibodies (1:2000 in the donkey serum blocking solution, Sigma-Aldrich F1804), overnight at 4°C, washed with PBS, and then incubated for 1 hour at room temperature with donkey secondary antibodies conjugated to 488 or 647 (Jackson ImmunoResearch) and 10 µg/mL Hoechst 33342 (Fischer Scientific BDB561908) in the donkey blocking solution before washing and mounting on slides with Immu-Mount (Thermo Fisher Scientific) and 1.5 mm coverslips (EMS).

Image Analysis

Images were acquired using a Zeiss Observer 7 inverted microscope equipped with a 63× oil-immersion objective (1.40 NA), LSM 800 confocal scanhead outfitted with an Airyscan superresolution detector controlled by Zen 5.0 software (Carl Zeiss Microscopy). Manipulation of images was limited to adjusting the brightness level, image size, rotation and cropping using FIJI (ImageJ, https://imagej.net/Fiji). Rod nucleus locations were measured using Imaris software (Bitplane). The 3D planes defining the bottom and top of the nuclear stack as well as the location of each nucleus of a FLAG-positive cell were chosen by hand and recorded. MATLAB (Mathworks) code was written to convert each nuclear location within the z-stack to its location between the two planes and then assigned a normalized value corresponding to the shortest distance to the plane defining the bottom of the nuclear stack. The MATLAB code is available at https://github.com/DrWessler/Disrupting-the-ciliary-gradient-of-active-Arl3-affects-rod-photoreceptor-nuclear-migration/. All phenotypes were measured using images taken from at least 3 independent retinas.

Cell culture

All cell culture experiments were performed using AD293 cells maintained at 37°C in 5% CO_2. Transient transfections were performed 1 day after seeding 1x10^{6} cells in a 10 cm plate and

experimental collection was performed 2 days after transfection. 5 µg of plasmid DNA was transfected per plate by incubating the DNA with 10 µg polyethyleneimine (Sigma, 408727) in serum free media for 10 min before being added dropwise to cells that had been changed to serum free media 1 hour prior.

Pull-downs

GST-PDEδ and GST alone were each expressed and purified from BL21(DE3) e. coli (NEB) after adding 0.25 mM IPTG for 4 hours at 28°C, lysing the cells (50 mM Tris pH 8, 50 mM NaCl, 5 mM $MgCl_2$, 5 mM BME, and cOmplete EDTA-free protease inhibitor (Millipore Sigma, 1183617001)), and eluting from a column with Ni-NTA beads (ThermoFisher, 88221) using 100 mM imidazole pH 8. GST-PDEδ (50 µg) was then crosslinked to 50 µL of magnetic glutathione beads (Sigma-Aldrich, G0924) using disuccinimidyl suberate (Thermo Scientific, 21555) and the beads were used to pulldown active Arl3 from AD293 cell lysates 48 hours after transient transfection with Arl3-FLAG mutants. Briefly, cells were lysed (20 mM Tris pH 7.5, 200 mM NaCl, 5mM $MgCl_2$, 0.5% Igepal (Fisher Scientific, AAJ19628AP), and cOmplete protease inhibitor cocktail), cleared by centrifugation at 14,000 x g for 10 min, incubated with GST beads for 10 min at 4°C, incubated with GST-PDEδ beads for 45 min at 4°C, washed with Buffer M (20 mM Tris pH 7.5, 5 mM MgCl2, 100 mM NaCl, 3 mM BME, 1% glycerol), and then heated to 55°C for 10 min in Laemmli sample buffer. When testing for the effect of Mg^{2+} and/or excess GTP on the amount of active Arl3, final concentrations of 10 mM EDTA or 65 mM $MgCl_2$ and/or 10 mM GTP were added to the lysate and vortexed before shaking at 30°C for 15 min. To stop the GTP loading in the presence of 10 mM EDTA, $MgCl_2$ to a final concentration of 65 mM was added before the pull-down.

In vivo *crosslinking and FLAG immunoprecipitations*

10 cm confluent plates of transiently transfected AD293 cells were washed well with PBS and then incubated in 1 mM disuccinimidyl suberate (Thermo Scientific, 21555) in PBS at 37°C for 10 min. The reaction was quenched by adding Tris Buffer pH 8, to a final concentration of 100 mM for 15 min at room temperature. After washing again with PBS, cells were collected and lysed in 50 mM Tris pH 7.5, 100 mM NaCl, 5 mM $MgCl_2$, 0.5% Igepal, 2% glycerol with cOmplete protease inhibitor cocktail. Immunoprecipitations were performed by adding 15 µL of magnetic FLAG beads (Sigma-Aldrich, M8823) to the lysates and rotating at 4°C for 2 hours before washing 3 times with a high salt buffer (50 mM Tris pH 7.5, 500 mM NaCl, 5 mM $MgCl_2$, 2% glycerol) and then eluting by shaking with 15 µL of 100 µg/µL of 3X FLAG peptide (Sigma-Aldrich, F4799) in the original lysis buffer for 30 min at 4°C.

Western blotting

SDS-PAGE using AnykD Criterion TGX Precast Midi Protein Gels (Bio-Rad) was followed by transfer at 90 mV for 90 minutes onto Immun-Blot Low Fluorescence PVDF Membrane (Bio-Rad). Membranes were blocked using Intercept Blocking Buffer (LI-COR Biosciences). The antibodies used for Western blotting were mouse anti-FLAG clone M2 (1:1000, Sigma-Aldrich F1804), polyclonal rabbit anti-Arl3 (1:1000, Novus Biologicals NBP1-88839), monoclonal anti-GFP JL-8 (1:1000, Clontech 632380), polyclonal rabbit anti-RP2 (1:1000, Sigma-Aldrich HPA000234), and monoclonal anti-MYC clone 9B11 (1:1000, Cell Signaling 2276S). Primary antibodies were diluted in 50% / 50% of Intercept / PBST and incubated overnight rotating at 4ºC. The next day, membranes were rinsed 3 times with PBST before incubating in the corresponding secondary donkey antibodies conjugated with Alexa Fluor 680 or 800 (LiCor Bioscience) in 50% / 50% / 0.02% of Intercept / PBST / SDS for 2 hours at 4ºC. Bands were visualized and quantified using the Odyssey CLx infrared imaging system (LiCor Bioscience). Images of the uncropped Western blots can be found in Supplemental Figure 1.

Mass Spectroscopy

Samples analyzed by mass spectroscopy were produced using the above protocols for transient transfection, *in vivo* crosslinking, and FLAG immunoprecipitation. After elution from the beads with 1X Laemmli sample buffer and brief gel electrophoresis, ~1x1mm gel pieces were subjected to reduction (20 mM DTT, 50 mM ammonium bicarbonate for 60oC for 15 min), alkylation (50 mM iodoacetamide SigmaUltra I1149 in 50 mM ammonium bicarbonate in the dark at RT for 1 hr), in-gel tryptic digestion (250 ng Trypsin-Lys-C mix Promega V5072 in 50 mM ammonium bicarbonate overnight at 37oC), and peptide extraction (0.2% trifluoroacetic acid in 50% acetonitrile at RT for 30 min). After drying by SpeedVac, the peptides were analyzed with a nanoAcquity UPLC system (Waters) coupled to an Orbitrap Q Exactive HF mass spectrometer (Thermo Fisher Scientific) employing the LC-MS/MS protocol in a data-independent acquisition mode. The peptides were separated on a 75-µm × 150-mm, 1.7-µm C18 BEH column (Waters) using a 90-min gradient of 8 to 32% of acetonitrile in 0.1% formic acid at a flow rate of 0.3 mL/min at 45 °C. Eluting peptides were sprayed into the ion source of the Orbitrap Q Exactive HF at a voltage of 2.0 kV. Progenesis QI Proteomics software (Waters) was used to assign peptides to the features and generate searchable files, which were submitted to Mascot (version 2.5) for peptide identification and searched against the UniProt reviewed mouse database (September 2019 release,17008 entrees). Only proteins with 2 or more peptides and protein confidence $P < 0.05$ were assigned as confidently identified.

Statistical analysis

To analyze the location of Arl3 mutant expressing rod nuclei, the skewness of the nuclei in each individual z-stack was calculated using Graphpad Prism. The pooled skewness values for each electroporation condition were then compared using a One-Way ANOVA and a significant difference ($p<0.0001$) was found among the means. Dunnett's multiple comparisons tests were then done to determine whether each condition had a significantly different nuclear localization skew than wild type Arl3-FLAG expressing rods. The skewness and p-value of the multiple comparison test for each condition are listed in Table 1.

For analysis of the amount of active Arl3 complexes formed in 293 cells expressing Arl3-FLAG mutants, the ~55kDa and ~45kDa bands were normalized to corresponding Arl3-Q71L-FLAG complex bands on the same gel. One-way ANOVA between D129N, Y90C, WT, and T31N showed a significant difference among the means ($p<0.0001$), and Tukey's multiple comparisons were performed.

FIGURES

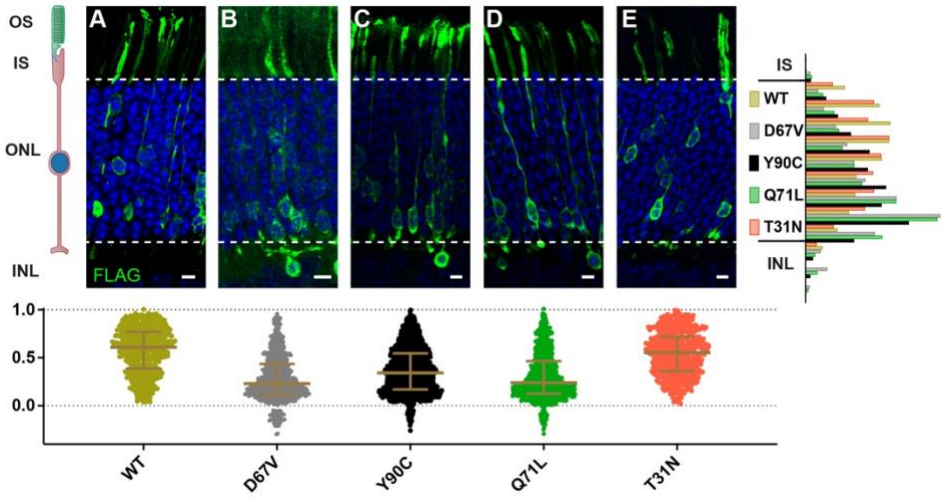

Fig. 1: Expression of dominant Arl3 mutants in rod photoreceptors causes nuclear mislocalization. Representative images showing cross-sections through wildtype mouse retinas electroporated with Arl3-3XFLAG (**A**), Arl3-D67V-FLAG (**B**), Arl3-Y90C-FLAG (**C**), Arl3-Q71L-FLAG (**D**), or Arl3-T31N-FLAG (**E**) and immunostained with anti-FLAG antibodies (green). Nuclei are counterstained with Hoechst (blue). Scale bars, 5 µm. Here and in all subsequent figures the nuclear position of electroporated rods is represented as follows: Below each image, a scatter plot shows the location of every Arl3-FLAG expressing nuclei, normalized to its position within the ONL with the apical edge set to 1.0 and the basal edge set to 0.0 (dashed lines in the images and graphs). Median and interquartile range are indicated in brown. To the right, a histogram shows the relative distribution of the nuclear position for each construct with nuclei sorted into 10 ONL and 3 INL bins. A minimum of 3 expressing eyes were analyzed for each construct. Abbreviations: outer segments (OS), inner segments (IS), outer nuclear layer (ONL), and inner nuclear layer (INL).

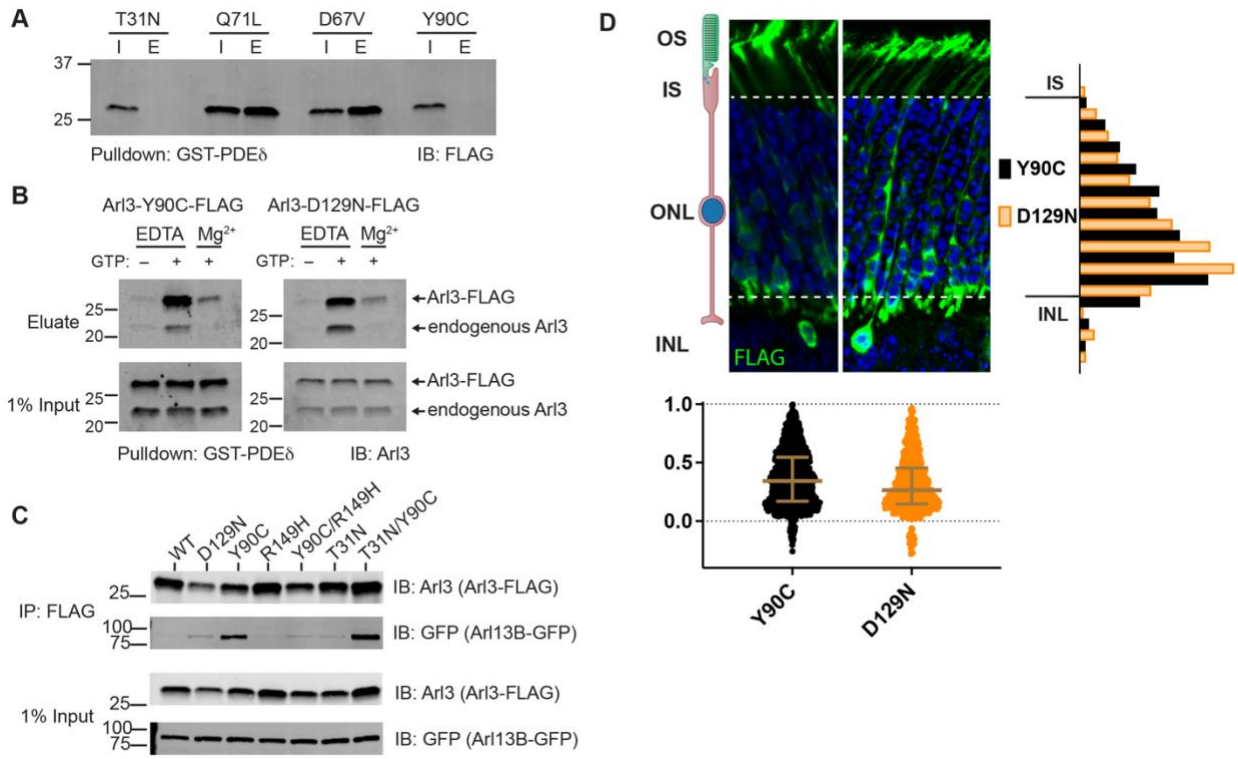

Fig. 2: Arl3-Y90C is a fast cycling GTPase. (**A**) 1% input (I) and eluates (E) from GST-PDEδ pulldowns using AD293 lysates expressing 3XFLAG-tagged Arl3 mutants immunoblotted with anti-FLAG antibodies. (**B**) Arl3-Y90C-FLAG or Arl3-D129N-FLAG lysates were incubated with 10 mM EDTA and/or 10 mM GTP, spiked with Mg^{2+}, and precipitated with GST-PDEδ. Westerns immunoblotted for Arl3 with eluates shown on top, and 1% inputs shown below. Arl3-FLAG and endogenous Arl3 bands labelled. (**C**) FLAG immunoprecipitation from AD293 lysates expressing Arl13B-GFP and Arl3-FLAG mutants. Westerns immunoblotted for Arl3 and GFP with 1% inputs shown on top and FLAG eluates on bottom. (**D**) Representative retinal cross-sections from Arl3-Y90C-FLAG or Arl3-D129N expressing rod photoreceptors stained with anti-FLAG antibodies (green) and counterstained with Hoechst (blue). Scale bars, 5 µm. Nuclear position of electroporated rods represented as described in Fig. 1.

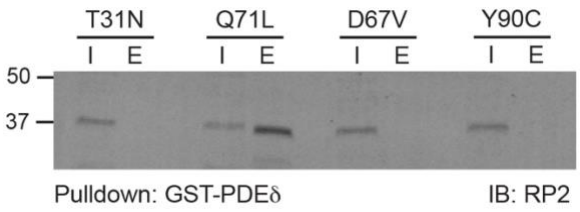

Fig. 2-SupFig 1: Unlike Arl3-Q71L, Arl3-D67V does not form a complex with RP2 and PDEδ. 1% input (I) and eluates (E) from GST-PDEδ pulldowns using AD293 lysates expressing 3XFLAG-tagged Arl3 mutants immunoblotted with anti-RP2 antibodies.

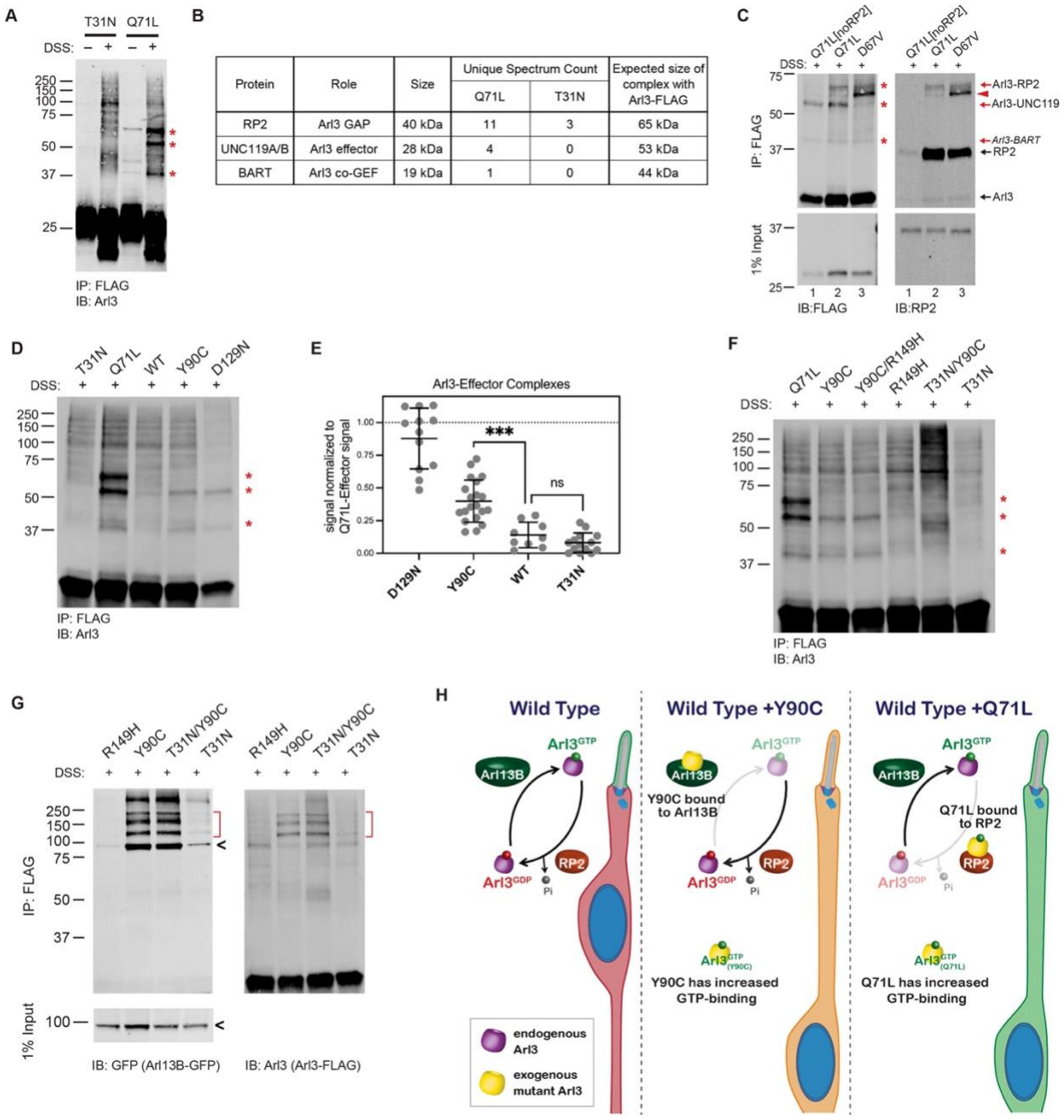

527

528 **Fig. 3: Arl3-Y90C undergoes GEF-independent activation in cell culture.** (**A**) FLAG
529 immunoprecipitation from DSS-crosslinked or non-crosslinked AD293 cell lysates expressing
530 either Arl3-T31N-FLAG or Arl3-Q71L-FLAG immunoblotted with anti-Arl3 antibodies. Red
531 asterisks indicate the three prominent bands that appear in crosslinked cells expressing Arl3-
532 Q71L-FLAG. (**B**) Table displaying the Arl3 binding partners identified by mass spectroscopy of
533 FLAG immunoprecipitations from either Arl3-Q71L-FLAG or Arl3-T31N-FLAG lysates after DSS
534 crosslinking. (**C**) Crosslinked FLAG immunoprecipitation from either Arl3-Q71L/E164A/D168A-

FLAG (Q71L[noRP2]), Arl3-Q71L-FLAG, or Arl3-D67V-FLAG probed with either anti-FLAG or anti-RP2 antibodies. Red asterisks and red arrows indicate crosslinked Arl3 complexes, red arrowhead indicates an additional FLAG and RP2 positive band present with D67V. Black arrows indicate the non-crosslinked proteins. (**D**) Representative Western blot showing crosslinked FLAG immunoprecipitation from Arl3-FLAG mutants: T31N, Q71L, Y90C, D129N. Red asterisks indicate the three crosslinked Arl3 complexes identified from Arl3-Q71L. (**E**) The signal intensity of crosslinked Arl3 complexes for each mutant normalized to the intensity of Arl3-Q71L complexes on the same blot. ns, p=0.8108 and ***, p=0.0007. (**F**) Crosslinked FLAG immunoprecipitation from Arl3-FLAG double-mutants and controls. Red asterisks indicate the three bands that appear in the presence of Arl3-Q71L. (**G**) Crosslinked FLAG immunoprecipitation from lysates expressing both Arl13B-GFP and Arl3-FLAG mutants. The red brackets identify Arl13B-Arl3 complexes and the black arrowheads non-crosslinked Arl13B-GFP. (**H**) Cartoon model depicts Arl3 GTPase cycle in rod photoreceptors under wild type conditions and how it is disrupted in the presence of exogenous Arl3-Y90C or Arl3-Q71L. Red indicates presence of inactive Arl3-GDP, green indicates presence of active Arl3-GTP, and orange indicates a mixed population of Arl3-GDP/Arl3-GTP.

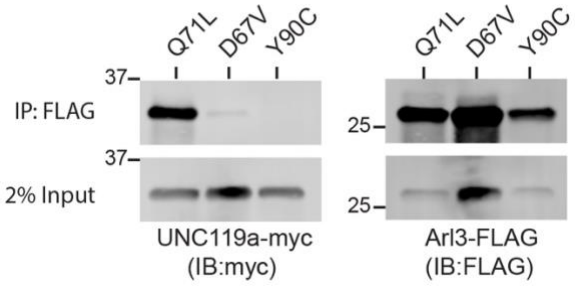

Fig. 3-SupFig 1: Unlike Arl3-Q71L, Arl3-D67V does not bind UNC119A. FLAG immunoprecipitations using AD293 lysates co-expressing 3XFLAG-tagged Arl3 mutants and myc-tagged UNC119a immunoblotted with anti-myc or anti-FLAG antibodies.

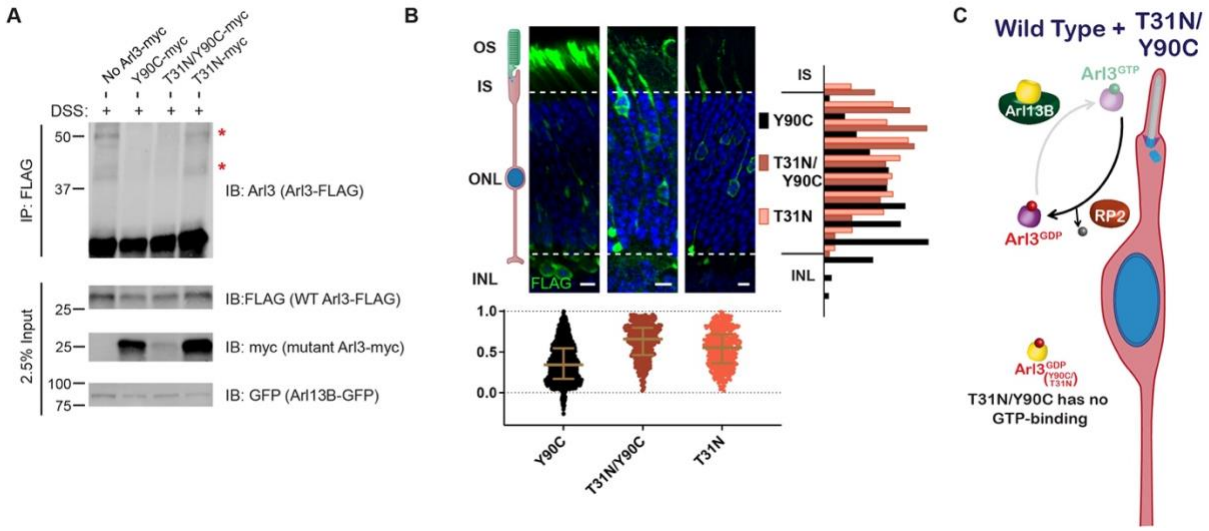

Fig. 4: Aberrant Arl3 activity drives the rod nuclear migration phenotype. (**A**) Crosslinked FLAG immunoprecipitation from AD293 lysates expressing Arl13B-GFP, wild type Arl3-FLAG, and myc-tagged Arl3 mutants. Red asterisks indicate the two crosslinked Arl3 complexes that appear in the presence of Arl3-Y90C. (**B**) Representative retinal cross-sections from Arl3-Y90C-FLAG, Arl3-T31N/Y90C-FLAG, or Arl3-T31N-FLAG expressing rod photoreceptors stained with anti-FLAG antibodies (green) and Hoechst (blue). Scale bars, 5 µm. Nuclear position of electroporated rods represented as described in Fig. 1. (**C**) Cartoon model portraying disrupted Arl3 GTPase cycle in rod photoreceptors in the presence of exogenous Arl3-T31N/Y90C mutant (yellow). Red indicates Arl3 is inactive throughout the rod and nuclear positioning is normal.

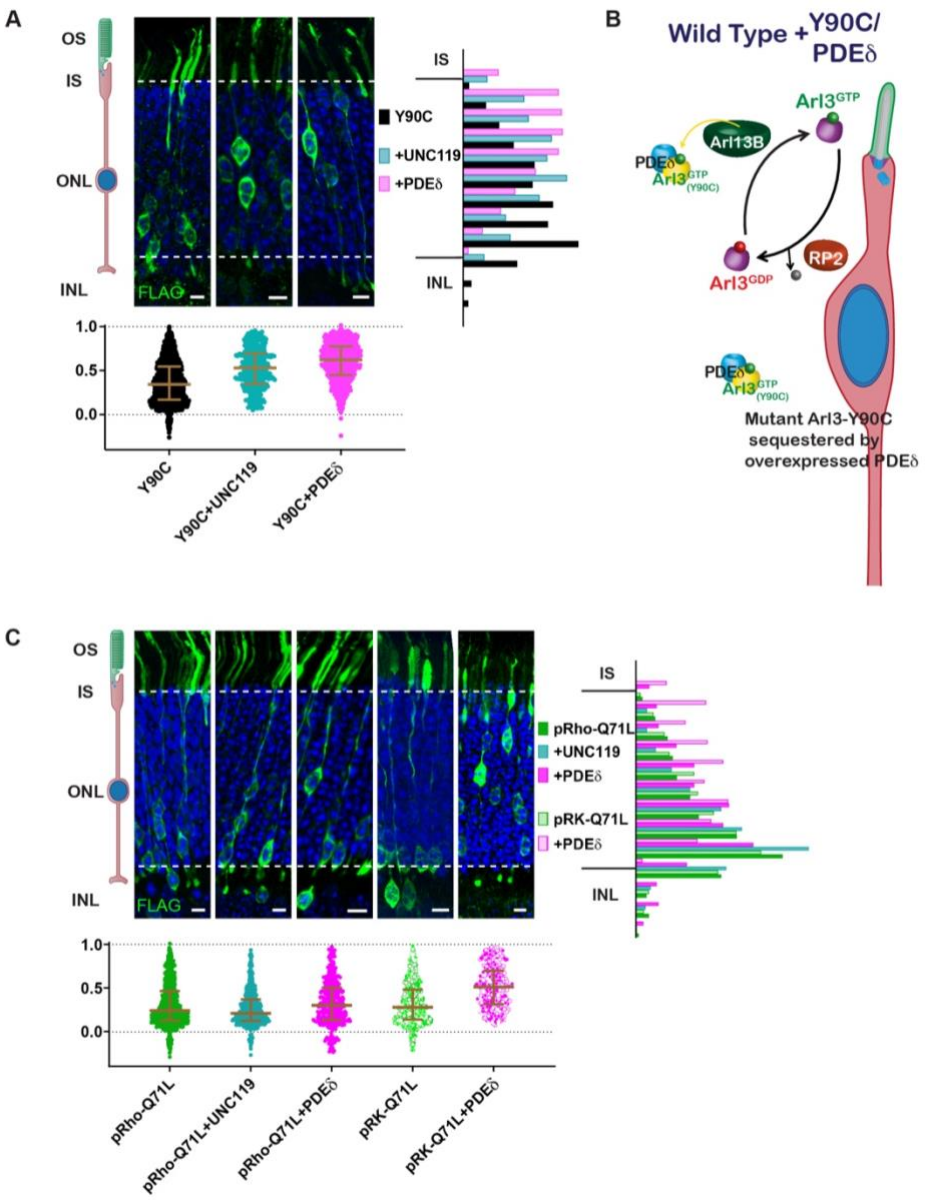

Fig. 5: Arl3 driven nuclear migration defects are rescued by overexpressing Arl3 effectors in rods. (**A**) Representative retinal cross-sections from Arl3-Y90C-FLAG co-expression with either the Arl3 effectors UNC119a or PDEδ. (**B**) Cartoon model illustrating the impact of Arl3 effector expression in the presence of Arl3-Y90C-FLAG in rod photoreceptors. Arl3 effectors reduce active Arl3 levels by sequestering Arl3-GTP. The ciliary Arl3-GTP gradient is restored allowing for normal nuclear positioning. (**C**) Representative retinal cross-sections from high (pRho) or low (pRK) Arl3-Q71L-FLAG co-expressed with either the Arl3 effectors UNC119a or PDEδ. FLAG (green) and Hoechst (blue). Scale bars, 5 µm. Nuclear position of electroporated rods represented as described in Fig. 1.

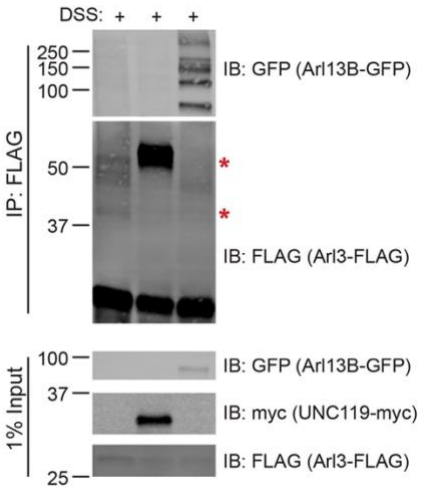

Fig. 5-SupFig 1: Co-expression of UNC119a or Arl13B-GFP decreases Arl3-Y90C-FLAG activity in cells. Crosslinked FLAG immunoprecipitation from AD293 lysates co-expressing Arl3-Y90C-FLAG with either myc-tagged UNC119a or Arl13B-GFP.

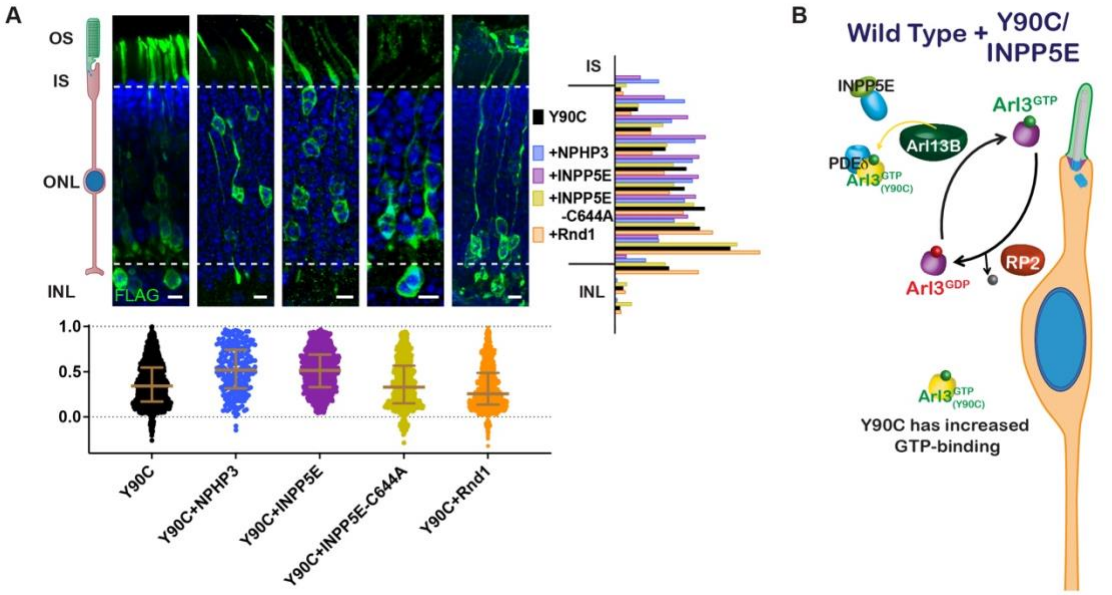

Fig. 6: Arl3-Y90C migration defect is rescued by overexpressing lipidated cargos destined for the cilium. (**A**) Representative retinal cross-sections from Arl3-Y90C-FLAG co-expression with different lipidated cargos: NPHP3, INPP5E or non-lipidated INPP5E-C644A (see Fig6-Sup1), and Rnd1 (a PDEδ cargo, see Fig6-Sup1). FLAG (green) and Hoechst (blue). Scale bars, 5 µm. Nuclear position of electroporated rods represented as described in Fig. 1. (**B**) Cartoon model illustrating the impact of ciliary lipidated cargo expression in the presence of Arl3-Y90C-FLAG in rod photoreceptors. Specific delivery cargos to the cilium causes a sufficient local enrichment of Arl3 effector (e.g., PDEδ) for removal of Arl3-Y90C from Arl13B. Even with the presence of aberrant Arl3-Y90C-GTP in the rod cell body (orange) restoration of the endogenous Arl3 (purple) GTPase cycle allows for normal nuclear positioning.

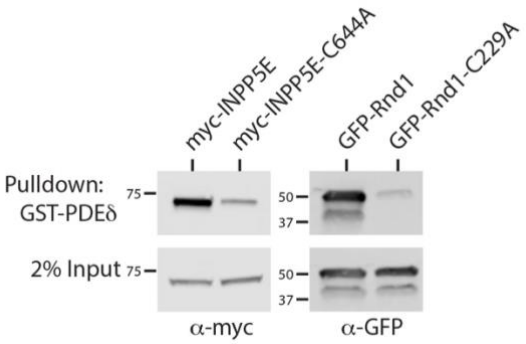

Fig. 6-SupFig 1: Lipid-dependent binding of INPP5E and Rnd1 to PDEδ. GST-PDEδ pulldowns using AD293 lysates expressing myc-tagged INPP5E and non-lipidated C644A mutant INPP5E immunoblotted with anti-RP2 antibodies. GST-PDEδ pulldowns using AD293 lysates expressing GFP-tagged Rnd1 and non-lipidated C229A mutant Rnd1 immunoblotted with anti-GFP antibodies.

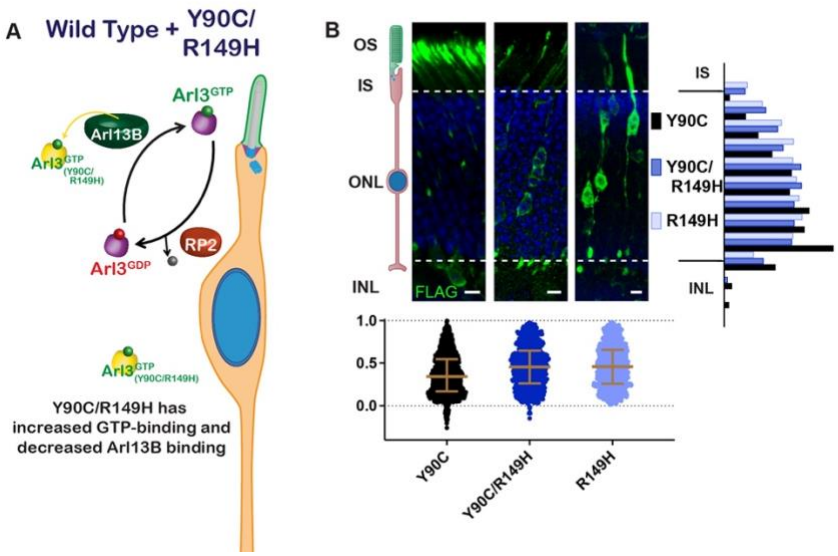

Fig. 7: Restoring the endogenous Arl3 cycle is sufficient for normal nuclear migration in the presence of aberrant Arl3 activity. (**A**) Cartoon model depicts the Arl3 GTPase cycle in rod photoreceptors in the presence of Arl3-Y90C/R149H. Endogenous Arl3 (purple) can restore the Arl3-GTP ciliary gradient (green) even in the presence of aberrant Arl3-Y90C/R149H-GTP in the rod cell body (orange). (**B**) Representative retinal cross-sections from Arl3-Y90C-FLAG, Arl3-Y90C/R149H-FLAG, or Arl3-R149H-FLAG expressing rod photoreceptors. FLAG (green) and Hoechst (blue). Scale bars, 5 µm. Nuclear position of electroporated rods represented as described in Fig. 1.

Arl3 mutant	co-expression	neuronal migration defect	skew	p value*	nucleotide binding properties	ref	human disease	ref
wild type		no	-0.2232		GEF Arl13B / GAP RP2	*Gotthardt K et al., 2015; Veltel S et al., 2008b*		
T31A		unknown			unknown		compound RD	*Fu L et al., 2021*
T31N		no	-0.1866	0.9997	no GTP binding	*Linari M et al., 1999*	n/a	
T31N/Y90C		no	-0.4093	0.8193	no GTP binding	this paper	n/a	
D67V		yes	0.5818	<0.0001	active w/ select effector binding	this paper	dominant RD	*Ratnapriya R et al., 2021*
Q71L		yes	0.6195	<0.0001	no GTP hydrolosis	*Linari M et al., 1999; Veltel S et al., 2008b*	n/a	
	+UNC119	yes	0.8616	<0.0001				
	+PDEd	yes	0.4449	0.0037				
pRK-Q71L		yes	0.5328	<0.0001	no GTP hydrolosis	*Linari M et al., 1999; Veltel S et al., 2008b*	n/a	
	+PDEd	no	0.1224	0.4546				
Y90C		yes	0.3053	0.0002	fast-cycling	this paper	dominant RD	*Strom SP et al., 2016; Holtan JP et al., 2019*
	+UNC119	no	-0.0898	0.995				
	+PDEd	no	-0.4235	0.3665				
	+NPHP3	no	-0.2929	0.9994				
	+INPP5E	no	-0.0367	0.7673				
	+INPP5E-C644A	yes	0.2357	0.0055				
	+Rnd1	yes	0.5827	<0.0001				
Y90C/R149H		no	0.0987	0.0921	fast-cycling	this paper	n/a	
R99I		unknown			unknown		recessive RD	*Sheikh SA et al., 2019*
C118F		unknown			unknown		compound RD	*Fu L et al., 2021*
D129N		yes	0.2855	0.0113	fast-cycling	Gotthardt K et al., 2015	n/a	
R149H		no	0.1229	0.051	no GEF binding	*Alkanderi S et al., 2018*	recessive RD	*Alkanderi S et al., 2018*

607 * significant difference from wild type using a Dunnett's multiple comparisons test

608 **Table 1: Summary of Arl3 mutants.** Human retinal phenotypes, GTPase function, mouse rod
609 nuclear migration defect and statistics are detailed with references listed.

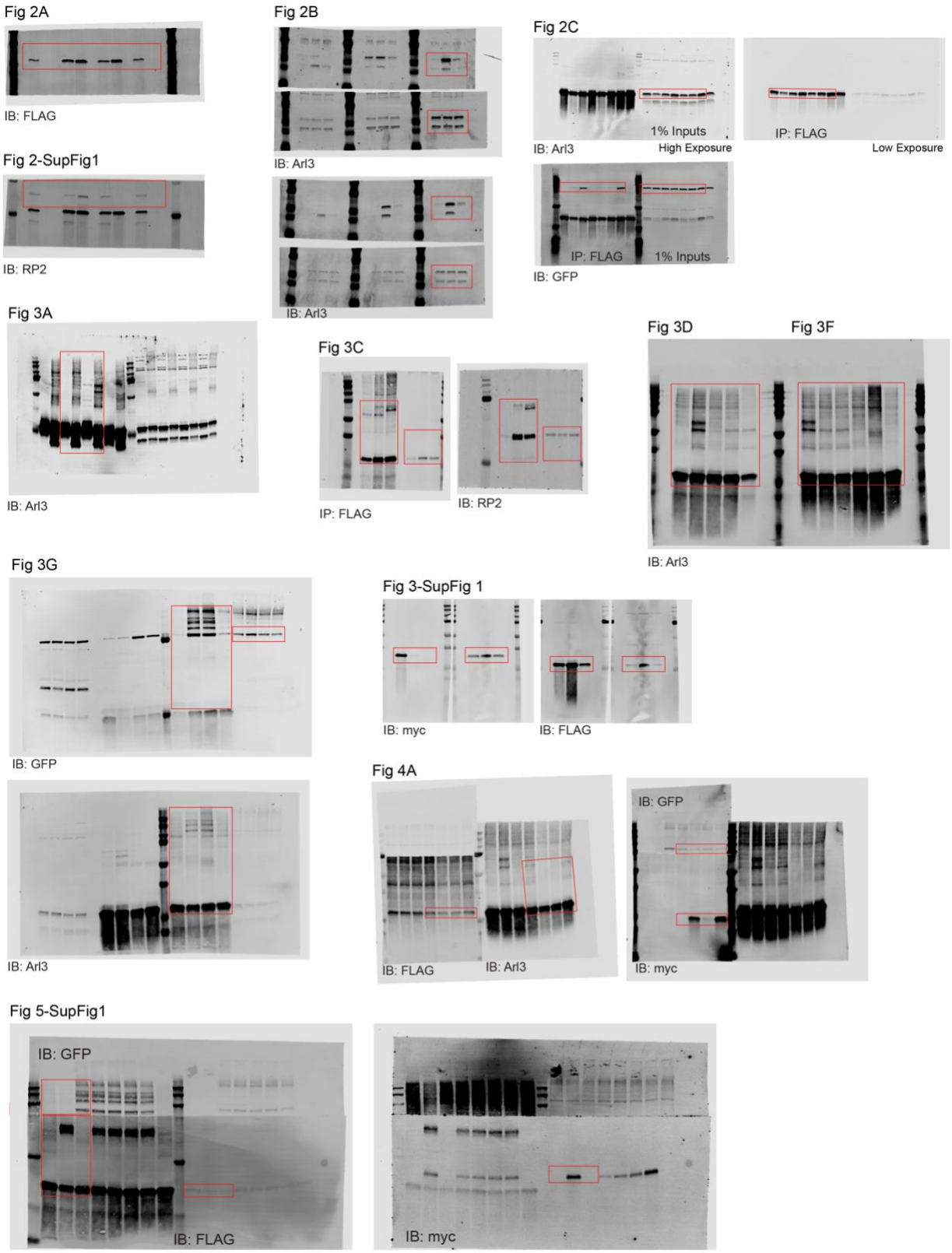

Supplementary Fig 1: Uncropped Western blot images.

Primer Name	Sequence (from 5' to 3')	Use
AgeI-hArl3	TATATATATAACCGGTGCCGCCACCATGGGCT	PCR Arl3 from pDEST47-Arl3
hArl3-KpnI	GGCCCTAGGTACCGCTTTCTTCTTTGCATTG	PCR Arl3 from pDEST47-Arl3
hArl3-T31N-F	ATAATGCTGGCAAGAACACTCTTCTGAAGCA	PCR mutagenesis
hArl3-T31N-R	TGCTTCAGAAGAGTGTTCTTGCCAGCATTAT	PCR mutagenesis
hArl3-D67V-F	AACTGAATGTATGGGTCATTGGTGGACAGAG	PCR mutagenesis
hArl3-D67V-R	CTCTGTCCACCAATGACCCATACATTCAGTT	PCR mutagenesis
hArl3-Q71L-F	GGGACATTGGTGGACTGAGGAAAATCAGACC	PCR mutagenesis
hArl3-Q71L-R	GGTCTGATTTTCCTCAGTCCACCAATGTCCC	PCR mutagenesis
hArl3-Y90C-F	GGAAGAATTATTTTGAAAATACCGATATTCTTATATGTGTAATCGACAGTGCAGACAGAAAAAGATTTGAAGA	PCR mutagenesis
hArl3-Y90C-R	TCTTCAAATCTTTTTCTGTCTGCACTGTCGATTACACATATAAGAATATCGGTATTTTCAAAATAATTCTTCC	PCR mutagenesis
hArl3-D129N-F	CTCATCTTTGCTAATAAGCAGAATTTGCTCACAGCAGCCCCT	PCR mutagenesis
hArl3-D129N-R	AGGGGCTGCTGTGAGCAAATTCTGCTTATTAGCAAAGATGAG	PCR mutagenesis
hArl3-R149H-F	CTGCATACCATCCACGACCGAGTCTG	PCR mutagenesis
hArl3-R149H-R	CAGACTCGGTCGTGGATGGTATGCAG	PCR mutagenesis
hArl3-E164AD168A-F	TCAGCTCTCACAGGAGCGGGCGTTCAGGCTGGCATGAACTGGGTC	PCR mutagenesis
hArl3-E164AD168A-R	GACCCAGTTCATGCCAGCCTGAACGCCCGCTCCTGTGAGAGCTGA	PCR mutagenesis
ecT4dC-hPDE6D	GTGGTAGTCTTATGTCAGCCAAGGACGAG	PCR PDEd from Dharmacon MHS6278-202829730
hPDE6D-HindIII	GCGCGCAAGCTTTCATCAAACATAGAAAAG	PCR PDEd from Dharmacon MHS6278-202829730
GSThPDE6D-F	CTGGTTCCGCGTGGTAGTATTATGTCAGCCAAGGACGAG	PCR PDEd from Dharmacon MHS6278-202829730
GSThPDE6D-R	GGCCGCAAGCTTCGTCATCATCATCAAACATAGAAAAGTCTCACTCTG	PCR PDEd from Dharmacon MHS6278-202829730
AgeI-UNC119a-F	CCCGGGATCCACCGGTGCCGCCACCATGAAGGTGAAGAAAG	PCR UNC119A from Origene RC203758
UNC119a-T2A-F	ATTCCTACAGTGGGACACCCAAAAAGCTTGAGGGCAGAGG	PCR UNC119A from Origene RC203758
UNC119a-T2A-R	CCTCTGCCCTCAAGCTTTTTGGGTGTCCCACTGTAGGAAT	PCR UNC119A from Origene RC203758
KpnI-UNC119-R	GTCGACTGGTACCGCGGGTGTCCCACTGTAG	PCR UNC119A from Origene RC203758
hNPHP3-Seq-F1	CTTCAAGTCCACTGGCTCGT	Sequencing human NPHP3
hNPHP3-Seq-F2	CAAGAGGGAGTTGGAGAGCA	Sequencing human NPHP3
hNPHP3-Seq-F3	GAAAAACCCTGAAGGAAAACC	Sequencing human NPHP3
hNPHP3-Seq-F4	CCAGCTCAGAGTCCTCCTTG	Sequencing human NPHP3
hNPHP3-Seq-F5	CTGCACTCTATCCGGGAGTC	Sequencing human NPHP3
hNPHP3-Seq-F6	ACAAAAGTGCAATGGCAACA	Sequencing human NPHP3
hNPHP3-Seq-F7	GATAATGCTCGGACCCTCAA	Sequencing human NPHP3
hNPHP3-Seq-F8	GCATCCTCGAGTTGGAGAAA	Sequencing human NPHP3
hNPHP3-Seq-R1	GCTTTTCCACCCAAGAGTGA	Sequencing human NPHP3
hNPHP3-Seq-R2	ACTCCTGGTTCTTGCTGACG	Sequencing human NPHP3
AgeI-hNPHP3-F	GATCCACCGGTGCCGCCACCATGGGGACCGCCTCGTCGCT	PCR NPHP3 from GeneCopoeia GC-H2370
hNPHP3-NotI-R	GGAGTGCGGCCGCCTACTTGTCATCGTCATCCTTGTAATCCCTTTGTCCTTGCTGAAGGA	PCR NPHP3 from GeneCopoeia GC-H2370
hNPHP3-MYC-R1	ATAAGCTTTTGTTCCCTTTGTCCTTGCTGAAGGA	Cloning myc tag onto NPHP3
hNPHP3-MYC-R2-NotI	AGGAGTGCGGCCGCCTACAGATCCTCTTCTGAGATAAGCTTTTGTTCCCT	Cloning myc tag onto NPHP3
mINPP5E-seqF2	TTGCAAGACTCAGTAGCCCA	Sequencing mouse INPP5E

Supplementary Table 1: Primer sequences and usage.

REFERENCES

Aghaizu, N.D., K.M. Warre-Cornish, M.R. Robinson, P.V. Waldron, R.N. Maswood, A.J. Smith, R.R. Ali, and R.A. Pearson. 2021. Repeated nuclear translocations underlie photoreceptor positioning and lamination of the outer nuclear layer in the mammalian retina. *Cell Rep*. 36:109461.

Alkanderi, S., E. Molinari, R. Shaheen, Y. Elmaghloob, L.A. Stephen, V. Sammut, S.A. Ramsbottom, S. Srivastava, G. Cairns, N. Edwards, S.J. Rice, N. Ewida, A. Alhashem, K. White, C.G. Miles, D.H. Steel, F.S. Alkuraya, S. Ismail, and J.A. Sayer. 2018. ARL3 Mutations Cause Joubert Syndrome by Disrupting Ciliary Protein Composition. *Am J Hum Genet*. 103:612-620.

Baker, S.A., M. Haeri, P. Yoo, S.M. Gospe, N.P. Skiba, B.E. Knox, and V.Y. Arshavsky. 2008. The outer segment serves as a default destination for the trafficking of membrane proteins in photoreceptors. *J Cell Biol*. 183:485-498.

Breuer, D.K., B.M. Yashar, E. Filippova, S. Hiriyanna, R.H. Lyons, A.J. Mears, B. Asaye, C. Acar, R. Vervoort, A.F. Wright, M.A. Musarella, P. Wheeler, I. MacDonald, A. Iannaccone, D. Birch, D.R. Hoffman, G.A. Fishman, J.R. Heckenlively, S.G. Jacobson, P.A. Sieving, and A. Swaroop. 2002. A comprehensive mutation analysis of RP2 and RPGR in a North American cohort of families with X-linked retinitis pigmentosa. *Am J Hum Genet*. 70:1545-1554.

Cantagrel, V., J.L. Silhavy, S.L. Bielas, D. Swistun, S.E. Marsh, J.Y. Bertrand, S. Audollent, T. Attié-Bitach, K.R. Holden, W.B. Dobyns, D. Traver, L. Al-Gazali, B.R. Ali, T.H. Lindner, T. Caspary, E.A. Otto, F. Hildebrandt, I.A. Glass, C.V. Logan, C.A. Johnson, C. Bennett, F. Brancati, T.I.J.S.R.D.S. International Joubert Syndrome Related Disorders Study Group, E.M. Valente, C.G. Woods, and J.G. Gleeson. 2008. Mutations in the cilia gene ARL13B lead to the classical form of Joubert syndrome. *Am J Hum Genet*. 83:170-179.

Cavenagh, M.M., M. Breiner, A. Schurmann, A.G. Rosenwald, T. Terui, C. Zhang, P.A. Randazzo, M. Adams, H.G. Joost, and R.A. Kahn. 1994. ADP-ribosylation factor (ARF)-like 3, a new member of the ARF family of GTP-binding proteins cloned from human and rat tissues. *J Biol Chem*. 269:18937-18942.

Cool, R.H., G. Schmidt, C.U. Lenzen, H. Prinz, D. Vogt, and A. Wittinghofer. 1999. The Ras Mutant D119N Is Both Dominant Negative and Activated. *Mol Cell Biol*. 19:6297-6305.

ElMaghloob, Y., B. Sot, M.J. McIlwraith, E. Garcia, T. Yelland, and S. Ismail. 2021. ARL3 activation requires the co-GEF BART and effector-mediated turnover. *eLife*. 10:e64624.

Evans, R.J., N. Schwarz, K. Nagel-Wolfrum, U. Wolfrum, A.J. Hardcastle, and M.E. Cheetham. 2010. The retinitis pigmentosa protein RP2 links pericentriolar vesicle transport between the Golgi and the primary cilium. *Hum Mol Genet*. 19:1358-1367.

Fansa, E.K., S.K. Kösling, E. Zent, A. Wittinghofer, and S. Ismail. 2016. PDE6δ-mediated sorting of INPP5E into the cilium is determined by cargo-carrier affinity. *Nat Commun*. 7:11366.

Fansa, E.K., and A. Wittinghofer. 2016. Sorting of lipidated cargo by the Arl2/Arl3 system. *Small GTPases*. 7:222-230.

Frederick, J.M., C. Hanke-Gogokhia, G. Ying, and W. Baehr. 2020. Diffuse or hitch a ride: how photoreceptor lipidated proteins get from here to there. *Biol Chem*. 401:573-584.

Fu, L., Y. Li, S. Yao, Q. Guo, Y. You, X. Zhu, and B. Lei. 2021. Autosomal Recessive Rod-Cone Dystrophy Associated With Compound Heterozygous Variants in. *Front Cell Dev Biol*. 9:635424.

Gotthardt, K., M. Lokaj, C. Koerner, N. Falk, A. Gießl, and A. Wittinghofer. 2015. A G-protein activation cascade from Arl13B to Arl3 and implications for ciliary targeting of lipidated proteins. *eLife*. 4:e11859.

Hanke-Gogokhia, C., Z. Wu, C.D. Gerstner, J.M. Frederick, H. Zhang, and W. Baehr. 2016. Arf-like Protein 3 (ARL3) Regulates Protein Trafficking and Ciliogenesis in Mouse Photoreceptors. *J Biol Chem*. 291:7142-7155.

Hanzal-Bayer, M., L. Renault, P. Roversi, A. Wittinghofer, and R.C. Hillig. 2002. The complex of Arl2-GTP and PDE delta: from structure to function. *EMBO J*. 21:2095-2106.

Higginbotham, H., T.-Y.Y. Eom, Laura E.E. Mariani, A. Bachleda, J. Hirt, V. Gukassyan, C.L. Cusack, C. Lai, T. Caspary, and E.S.S. Anton. 2012. Arl13b in primary cilia regulates the migration and placement of interneurons in the developing cerebral cortex. *Dev Cell*. 23:925-938.

Holopainen, J.M., C.L. Cheng, L.L. Molday, G. Johal, J. Coleman, F. Dyka, T. Hii, J. Ahn, and R.S. Molday. 2010. Interaction and localization of the retinitis pigmentosa protein RP2 and NSF in retinal photoreceptor cells. *Biochemistry*. 49:7439-7447.

Holtan, J.P., K. Teigen, I. Aukrust, R. Bragadóttir, and G. Houge. 2019. Dominant ARL3-related retinitis pigmentosa. *Ophthalmic Genet*. 40:124-128.

Ismail, S.A., Y.-X. Chen, M. Miertzschke, I.R. Vetter, C. Koerner, and A. Wittinghofer. 2012. Structural basis for Arl3-specific release of myristoylated ciliary cargo from UNC119. *EMBO J*. 31:4085-4094.

Khani, S.C., B.S. Pawlyk, O.V. Bulgakov, E. Kasperek, J.E. Young, M. Adamian, X. Sun, A.J. Smith, R.R. Ali, and T. Li. 2007. AAV-mediated expression targeting of rod and cone photoreceptors with a human rhodopsin kinase promoter. *Invest Ophthalmol Vis Sci*. 48:3954-3961.

Li, L., N. Khan, T. Hurd, A.K. Ghosh, C. Cheng, R. Molday, J.R. Heckenlively, A. Swaroop, and H. Khanna. 2013. Ablation of the X-linked retinitis pigmentosa 2 (Rp2) gene in mice results in opsin mislocalization and photoreceptor degeneration. *Invest Ophthalmol Vis Sci*. 54:4503-4511.

Linari, M., M. Hanzal-Bayer, and J. Becker. 1999. The delta subunit of rod specific cyclic GMP phosphodiesterase, PDEδ, interacts with the Arf-like protein Arl3 in a GTP specific manner. *FEBS Letters*. 458:55-59.

Matsuda, T., and C.L. Cepko. 2004. Electroporation and RNA interference in the rodent retina in vivo and in vitro. *Proc Natl Acad Sci USA*. 101:16-22.

Mookherjee, S., S. Hiriyanna, K. Kaneshiro, L. Li, Y. Li, W. Li, H. Qian, T. Li, H. Khanna, P. Colosi, A. Swaroop, and Z. Wu. 2015. Long-term rescue of cone photoreceptor degeneration in retinitis pigmentosa 2 (RP2)-knockout mice by gene replacement therapy. *Hum Mol Genet*. 24:6446-6458.

Pearring, J.N., E.C. Lieu, J.R. Winter, S.A. Baker, and V.Y. Arshavsky. 2014. R9AP targeting to rod outer segments is independent of rhodopsin and is guided by the SNARE homology domain. *Mol Biol Cell*. 25:2644-2649.

Pearring, J.N., W.J. Spencer, E.C. Lieu, and V.Y. Arshavsky. 2015. Guanylate cyclase 1 relies on rhodopsin for intracellular stability and ciliary trafficking. *eLife*. 4:e12058.

Ratnapriya, R., S.G. Jacobson, A.V. Cideciyan, M.A. English, A.J. Roman, A. Sumaroka, R. Sheplock, and A. Swaroop. 2021. A Novel ARL3 Gene Mutation Associated With Autosomal Dominant Retinal Degeneration. *Front Cell Dev Biol*. 9:720782.

Schrick, J.J., P. Vogel, A. Abuin, B. Hampton, and D.S. Rice. 2006. ADP-ribosylation factor-like 3 is involved in kidney and photoreceptor development. *Am J Pathol*. 168:1288-1298.

Sheikh, S.A., R.A. Sisk, C.R. Schiavon, Y.M. Waryah, M.A. Usmani, D.H. Steel, J.A. Sayer, A.K. Narsani, R.B. Hufnagel, S. Riazuddin, R.A. Kahn, A.M. Waryah, and Z.M. Ahmed. 2019. Homozygous Variant in ARL3 Causes Autosomal Recessive Cone Rod Dystrophy. *Invest Ophthalmol Vis Sci*. 60:4811-4819.

Sorokin, A.V., E.R. Kim, and L.P. Ovchinnikov. 2007. Nucleocytoplasmic transport of proteins. *Biochemistry*. 72:1439-1457.

Stoufflet, J., M. Chaulet, M. Doulazmi, C. Fouquet, C. Dubacq, C. Métin, S. Schneider-Maunoury, A. Trembleau, P. Vincent, and I. Caillé. 2020. Primary cilium-dependent cAMP/PKA signaling at the centrosome regulates neuronal migration. *Sci Adv*. 6:eaba3992.

Strom, S.P., M.J. Clark, A. Martinez, S. Garcia, A.A. Abelazeem, A. Matynia, S. Parikh, L.S. Sullivan, S.J. Bowne, S.P. Daiger, and M.B. Gorin. 2016. De Novo Occurrence of a Variant in ARL3 and Apparent Autosomal Dominant Transmission of Retinitis Pigmentosa. *PLoS One*. 11:e0150944.

Veltel, S., R. Gasper, E. Eisenacher, and A. Wittinghofer. 2008a. The retinitis pigmentosa 2 gene product is a GTPase-activating protein for Arf-like 3. *Nat Struct Mol Biol*. 15:373-380.

Veltel, S., A. Kravchenko, S. Ismail, and A. Wittinghofer. 2008b. Specificity of Arl2/Arl3 signaling is mediated by a ternary Arl3-effector-GAP complex. *FEBS Letters*. 582:2501-2507.

Weiner, M.P., G.L. Costa, W. Schoettlin, J. Cline, E. Mathur, and J.C. Bauer. 1994. Site-directed mutagenesis of double-stranded DNA by the polymerase chain reaction. *Gene*. 151:119-123.

Wright, Z.C., R.K. Singh, R. Alpino, A.F.X. Goldberg, M. Sokolov, and V. Ramamurthy. 2016. ARL3 regulates trafficking of prenylated phototransduction proteins to the rod outer segment. *Hum Mol Genet*. 25:2031-2044.

Yu, J., K. Lei, M. Zhou, C.M. Craft, G. Xu, T. Xu, Y. Zhuang, R. Xu, and M. Han. 2011. KASH protein Syne-2/Nesprin-2 and SUN proteins SUN1/2 mediate nuclear migration during mammalian retinal development. *Hum Mol Genet*. 20:1061-1073.

Zhang, H., R. Constantine, S. Vorobiev, Y. Chen, J. Seetharaman, Y.J. Huang, R. Xiao, G.T. Montelione, C.D. Gerstner, M.W. Davis, G. Inana, F.G. Whitby, E.M. Jorgensen, C.P. Hill, L. Tong, and W. Baehr. 2011. UNC119 is required for G protein trafficking in sensory neurons. *Nat Neurosci*. 14:874-880.

Zhang, H., X.-h. Liu, K. Zhang, C.-K. Chen, J.M. Frederick, G.D. Prestwich, and W. Baehr. 2004. Photoreceptor cGMP phosphodiesterase delta subunit (PDEdelta) functions as a prenyl-binding protein. *J Biol Chem*. 279:407-413.